

## **Author Manuscript**

**Title:** Key Features of Polyimide-Derived Carbon Molecular Sieves

**Authors:** William J. Koros, Prof.; Wulin Qiu; Johannes Leisen; Zhongyun Liu; Wenying Quan

This is the author manuscript accepted for publication. It has not been through the copyediting, typesetting, pagination and proofreading process, which may lead to differences between this version and the Version of Record.

**To be cited as:** 10.1002/anie.202106740

**Link to VoR:** <https://doi.org/10.1002/anie.202106740>

# Key Features of Polyimide-Derived Carbon Molecular Sieves

Wulin Qiu,<sup>[a]</sup> Johannes E Leisen,<sup>[b]</sup> Zhongyun Liu,<sup>[a]</sup> Wenying Quan,<sup>[a]</sup> William J Koros<sup>\*[a]</sup>

[a] Dr. W. Qiu, Dr. Z. Liu, Dr. W. Quan, Prof. Dr. W. J. Koros,  
School of Chemical and Biomolecular Engineering  
Georgia Institute of Technology  
Atlanta, GA 30332-0100, USA  
E-mail: [wjk@chbe.gatech.edu](mailto:wjk@chbe.gatech.edu)

[b] Dr. J. E. Leisen  
School of Chemistry and Biochemistry  
Georgia Institute of Technology  
Atlanta, GA 30332-0400, USA

Supporting information for this article is given via a link at the end of the document.

**Abstract:** Carbon molecular sieve (CMS) membranes have impressive separation properties; however, both chemical and morphology structures need to be understood better. Here we characterize CMS with the simplest polyimide (PI) PMDA/pPDA (PMDA=Pyromellitic Dianhydride, pPDA=p-Phenylenediamine), using FTIR, solid state <sup>15</sup>N-NMR, <sup>13</sup>C-NMR, XPS, XRD, and Raman spectra to study chemical structure. We also compare gas separation properties for this CMS to a CMS derived from a more conventional PI precursor. The detailed characterization shows the presence of aromatic pyridinic, pyrrolic rings as well as graphitic, pyridonic components and a few other groups in both CMS types derived from the very different precursors. The CMS morphologies, while related to precursor and pyrolysis temperature details, show similarities consistent with a physical picture comprising distributed molecular sieving plate-like structures. These results assist in understanding diverse CMS membrane separation performance.

## Introduction

Carbon molecular sieve (CMS) membranes<sup>[1]</sup> have gained attention due to their excellent thermal, chemical, and plasticization stability, and particularly attractive gas separation properties,<sup>[1e, 1i, 1j]</sup> which surpass the permeability versus selectivity "polymer upper bound" trade-off.<sup>[3]</sup> CMS membranes can be created by pyrolysis of polyimide precursor membranes under controlled conditions to produce relatively pure carbon materials. During pyrolysis random coil precursor polymers become aromatized by releasing small molecules to form rigid highly aromatic "strands". Evidence indicates that such strands can organize into imperfect "plates", and neighboring plates further organize to form imperfect "cell" structures. Adjacent "cells" can coalesce to form a larger "cellular" structure with 7-20 Å internal micropore volumes having ultramicropore cell walls,<sup>[4]</sup> with "orphan strands" randomly packed between cells to form a continuous phase around "cells" in the "cellular" structure,<sup>[5]</sup> as illustrated in Figure 1. Besides small "normal" ultramicropores (<7 Å) between "strands" in individual "plates", imperfections at the plate joints can create "slit bypass pores".<sup>[6]</sup> The envisioned slit-like pore structure of amorphous CMS, with large micropores connected by smaller ultramicropores windows, provides unique properties due to a bimodal pore distribution.<sup>[2b, 4, 6-7]</sup> The combination of micropores and ultramicropores provide both high

flux and high efficiency in gas separations via a molecular sieving function.

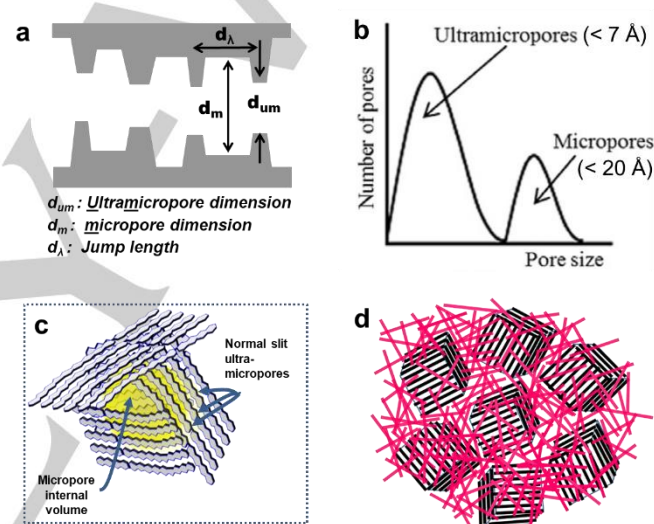


**Figure 1.** CMS membrane with (a) Ideal "slit-like" pore structure, (b) Bimodal distribution of pores, (c) Idealized micropore "cell" with ultramicropores between "strands" in the plate, and (d) Cellular structure composed with multiple micropore "cells" with ultramicropore walls surrounded by continuous phase of randomly dispersed "strands" not included in plate (shown in red to distinguish from strands in plate) believed to reflect the CMS morphology resulting from pyrolysis of conventional random coil polyimide precursors.

The ultramicropores, between the carbon-rich "strands", largely determine the CMS gas separation selectivity, so studying the chemically-relevant "strand" structure can help understand the ultramicropore structure as well as defects within and between plates. Such information can help understand CMS membranes and their aging and separation behaviors. Chemically-relevant strand structure can also test formation mechanisms described above that affect tuning of ultramicropores and micropores for separation of specific gas pairs. Polyimides have been shown to be a diverse family of precursors to make CMS membranes for gas separation.<sup>[2a, 2b, 2d-j]</sup> In order to understand such precursors, the structurally simplest PI, PMDA/pPDA (Scheme S1) was synthesized using <sup>15</sup>N-labeled diamine as precursor polymer. This PI was pyrolyzed under varied temperatures to create CMS materials. Solid state <sup>15</sup>N-NMR, and <sup>13</sup>C-NMR, XPS, and Raman spectra were used to analyze the nature of elements in the CMS, including C, N, and O to elucidate the hypothetical morphological

## RESEARCH ARTICLE

features. Gas separation properties of CMS membranes from PMDA/pPDA (w/o  $^{15}\text{N}$ ) were evaluated compared to CMS structures derived from a more conventional precursor to test the prevailing CMS model.

The  $^{15}\text{N}$  labeled PMDA/pPDA allowed investigating the detailed chemical structure of CMS materials. PMDA/pPDA has the simplest chemical structure in the polyimide family, therefore facilitating mechanistic studies of pyrolysis mechanisms for understanding more complex commonly used polyimides. Especially  $^{15}\text{N}$ -NMR of the labeled polymer allows the direct observation of structural changes of the imide ring at different stages in the pyrolysis.

## Results and Discussion

TGA and FTIR (Figure S1) indicate successful synthesis of the  $^{15}\text{N}$ -labeled PMDA/pPDA. This is confirmed by the solid-state NMR (Figure 2). Since both the PMDA/pPDA polyimide and CMSs are insoluble, high resolution solid-state magic angle spinning (MAS) NMR<sup>[8]</sup> is used. Basic principles of this technique rely upon rapid spinning of samples at an angle of 54.74 degree with respect to the magnetic field to average quantum mechanical interactions, which otherwise cause significant broadening of the detected NMR signal. For one part of this study we use the variable amplitude cross-polarization (VACP) technique, which is based on the transfer of magnetization from the  $^1\text{H}$  nuclei to the  $^{13}\text{C}$  or  $^{15}\text{N}$  nuclei. This techniques allows sensitive detection of  $^{13}\text{C}$  or  $^{15}\text{N}$  nuclei in the direct vicinity of  $^1\text{H}$ . We also use the direct polarization (DP) technique, which is based on the direct excitation of  $^{13}\text{C}$  or  $^{15}\text{N}$  nuclei. This technique allows the detection of all  $^{13}\text{C}$  or  $^{15}\text{N}$  sites irrespectively of their proximity to hydrogen atoms. In Figure 2a, the strong peak at 103.8 ppm in PAA is assigned to N atoms in  $-\text{CONH}-$  moieties, the small peak at 141.1 ppm is assigned to N atoms in imide ring of  $-\text{N}(\text{CO})_2-$  indicating a partial imidization of the PAA; the small peak at 14.0 ppm is assigned to N atoms in  $-\text{NH}_2$  end group of the polymer. In PI sample, the strong peak of N atoms in the imide ring shows at 144.4 ppm, and the very small peak at 94.4 ppm indicates trace amount of PAA in the PI. The small peak at 20.2 ppm is caused by the N atoms of the  $-\text{NH}_2$  end-group. In Figure 2b, peaks marked "ssb" are so called spinning side bands caused by the technically limited frequencies of MAS spinning. For PAA, the peak at 167.4 ppm is assigned to the C atom in  $\text{C}=\text{O}$  moiety, while the broad peaks at 120.6-134.2 ppm are associated with aromatic C atoms. The C atoms peak of  $\text{C}=\text{O}$  at 165 ppm (C1) in PI becomes narrow, and the aromatic C atoms peaks also get narrow and appear at 137 ppm (C2), 130 ppm (C3, C4), and 116 ppm (C5), as assigned in the polyimide chemical structure in Figure 2b. The chemical shift in solid polymers is associated with conformational disorder and therefore varying electronic environment experienced by individual  $^{13}\text{C}$  sites. The imidization to form rigid polymers, therefore greatly reduces conformational disorder of the PI, which in turn leads to narrower line-shapes.

As expected, CMSs showed quite different FTIR spectra from the precursor (Figure S1b). For PMDA/pPDA, the resulting CMS was found to maintain some degree of PI structure for pyrolysis temperature below 550°C. However, higher pyrolysis temperatures resulted in increased carbonization degrees, and CMS-675 and CMS-800 showed typical FTIR spectra of carbon materials. Solid-state NMR provided more detailed information on

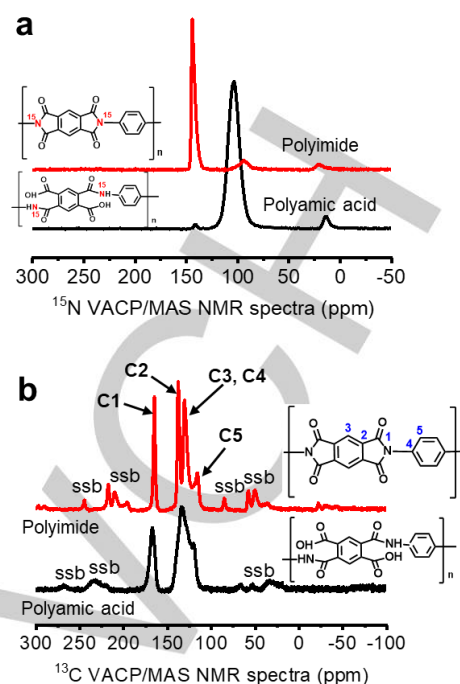


**Figure 2.** Solid-state NMR spectra of  $^{15}\text{N}$  labeled PMDA/pPDA polyamic acid (PAA) and polyimide (PI): (a)  $^{15}\text{N}$  VACP/MAS NMR, and (b)  $^{13}\text{C}$  VACP/MAS NMR.

CMS materials. For completely pyrolyzed PMDA/pPDA the VACP-MAS method will not detect any  $^{15}\text{N}$  sites, which is mostly due to the lack of hydrogen at the sites. However,  $^{15}\text{N}$  atoms existing at edges or defect sites are expected to be observable, since H atoms tend to exist at edges or within defects in graphitic plates of carbon materials. Because CMS-675 and CMS-800 were conductive, it was not possible to measure their NMR spectra. Only CMS-500 and CMS-550 were measured to identify the status of N atoms at edges or defect of the samples in Figure 3a. Peak intensities in CP-MAS spectra usually do not quantitatively correspond to molar concentrations. The strong peak at 144 ppm in CMS-500 in Figure 3a (N atoms within the imide ring), suggests that some PI structure is maintained in CMS-500; however, some degree of carbonization is likely. Overlapping peaks at 105 ppm, 92.5 ppm, and 82 ppm may be assigned to pyrrolic N atoms with different structures<sup>[9]</sup> and possibly also some N atoms in  $-\text{CONH}-$  moieties resulting from pyrolysis intermediates; the shoulders between 120 ppm to 130 ppm may be due to graphitic N atoms and pyrrolic N atoms;<sup>[9a]</sup> the small peak at 22 ppm is assigned to the N atoms of  $-\text{NH}_2$  end-group as found in PI. For CMS-550, the peak of imide ring (114 ppm) disappeared, while peaks of pyrrolic N atoms at 104 ppm and 82 ppm appear stronger; the shoulder peak at 138 ppm is assigned to graphitic N atom which is bonded to three carbon atoms; the broad weak peak at  $\sim 225$  to  $\sim 270$  ppm is assigned to pyridinic type N atoms with different structures.<sup>[9-10]</sup> The peak intensities qualitatively indicate that more N atoms exist as pyrrolic than as pyridinic species at the edge or as defect sites in CMS-500 and CMS-550. This fact is consistent with a 6FDA<sub>1</sub>:BPDA<sub>1</sub>/DAM<sub>2</sub> (Scheme S2) copolyimide derived CMS where it was found that strands comprising a typical ultramicropore-rich "plate" are mostly pyrrolic in nature.<sup>[11]</sup> As will be discussed later, the presence of pyridinic and pyrrolic N in the strands is apparent in all polyimide-derived CMS materials.

Due to sample conductivity, only CMS-500 and CMS-550 were successfully measured with  $^{13}\text{C}$  VACP/MAS NMR to identify C

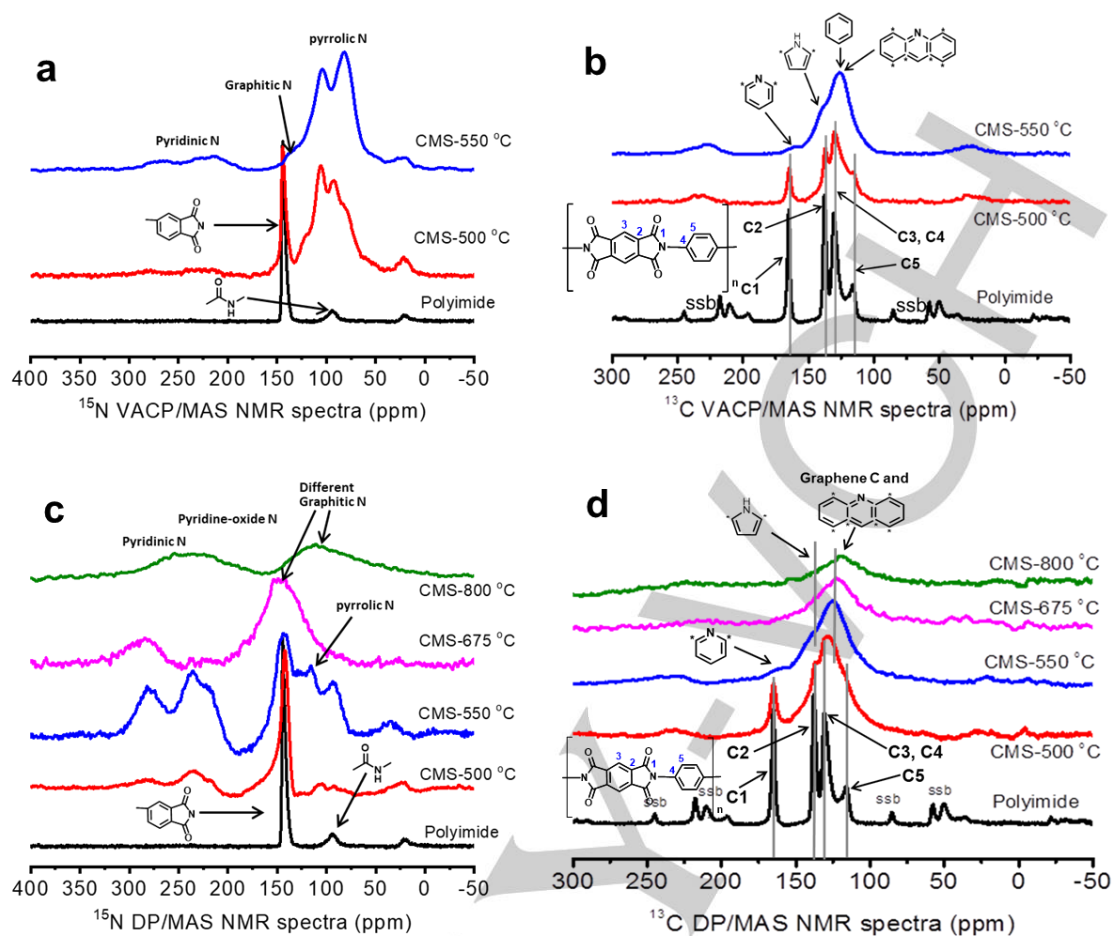


**Figure 3.** Solid-state NMR spectra of PMDA/pDA polyimide and CMS materials: (a)  $^{15}\text{N}$  VACP/MAS NMR, (b)  $^{13}\text{C}$  VACP/MAS NMR, (c)  $^{15}\text{N}$  DP/MAS NMR, and (d)  $^{13}\text{C}$  DP/MAS NMR (the \* indicates C atoms).

atoms that are associated with N atoms at edges or defects. Shown in Figure 3b, the  $^{13}\text{C}$  spectrum of the CMS-500 still contains sharp peaks, which coincide with those of PI. The peak at 165 ppm is assigned to the C atom of C=O, while peaks at 137 ppm, 130 ppm, and 116 ppm are associated with aromatic C atoms. However, overall a broadening of peaks, especially the aromatic moieties, is observed. In CMS-550, instead of the narrow peak at 165 ppm due to the C atom of C=O in imide rings, a broad weak peak is apparent at about 161 ppm, which is likely due to the  $\alpha$ -C atoms associated with pyridinic N atoms (noted with a "\*" in Figure 3b and in Figure 3d) as well as possibly some remaining C=O functional group.<sup>[9a]</sup> The broad peak between 150–100 ppm can be assigned to aromatic C atoms as well as to various fused aromatic ring structures. The peak at 126 ppm is assigned to aromatic carbon atoms,<sup>[9a, 12]</sup> and likely also from contribution of  $\beta$ -C atoms associated with pyridinic N atoms;<sup>[9a]</sup> the shoulder at about 139 ppm can also be assigned to the  $\alpha$ -C atoms associated with pyrrolic N atoms.<sup>[9a]</sup> Note that the broadening of lines is very typical for the generation of a graphitic structure.<sup>[12]</sup>

While the CP-MAS method provides a sensitive measurement of  $^{13}\text{C}$  or  $^{15}\text{N}$  sites in the proximity of hydrogen, the DP-NMR method detects nuclei irrespective of the presence of hydrogen, which makes it a valuable comparison tool. The DP method is less sensitive to tuning imperfections and the associated exact match of rf-power of both the  $^1\text{H}$  and the  $^{15}\text{N}$  or  $^{13}\text{C}$  channel. Therefore it is possible to record DP NMR spectra of CMS -675 and CMS-800. Figure 3c shows that, similar to PI sample, CMS-500 has a strong peak at 143 ppm, which is assigned to N atoms in the imide ring.

The broad small peaks at 200–300 ppm result from intermediate pyrolysis products including also kinds of pyridinic N atoms. The broad weak peak at about 100 ppm is probably caused by pyrrolic N atoms.<sup>[9]</sup> In the CMS-550, the peaks appearing in CMS-500 still exist, indicating CMS-550 has similar N atoms as in CMS-500; hence, so features of the polymer structure are partially retained in CMS-550. However, a broadening of peaks is an indication for a higher carbonization degree than CMS-550.<sup>[12]</sup> The broader peak at 143 ppm is due to the graphitic N atoms as well as N atoms within the pyrolyzed polymeric intermediates of bulk materials; the peak at 116 ppm is assigned to pyrrolic N atoms, and the peak at 93 ppm to pyrrolic N atoms as well as N atoms in the -CO-N- structure due to imide ring opened in pyrolysis. Similar to the CMS-500, the broad peak at 200–300 ppm is assigned to pyridinic N atoms in intermediates. The CMS-675 showed a significantly different NMR spectrum from CMS-550; peaks attributed to the polymer have now completely disappeared leaving only two broad peaks. The peak of pyridinic N atoms at 284 ppm is evident. The strong broad peak at 148 ppm can be assigned to graphitic N atoms of different structures and pyrrolic N atoms. Only two very broad peaks are observed for the CMS-800. The peak between 170 to 310 ppm is due to pyridinic N atoms and likely also due to pyridine-oxide N atoms; the peak between 50 to 150 ppm is assigned to different structures found within graphitic N atoms as well as pyrrolic N atoms. The shift of these two broad peaks to lower ppm values has been previously observed for carbon materials, which were produced by a controlled pyrolysis; it was attributed to the increased formation of

graphitic microcrystallites.<sup>[12]</sup> Peak intensities in DP spectra only quantitatively correspond to the concentration of corresponding moieties if  $T_1$ -relaxation of all sites is complete. The pyrolysis is expected to introduce an environment containing sufficient paramagnetic defects to lead to short  $T_1$ -relaxation times such that quantitative conditions for the DP spectrum are likely. Hence results indicate that more N atoms exist as graphitic forms at higher pyrolysis temperature.

Shown in Figure 3d, CMS-500 still has the peak at 165 ppm due to C atom of C=O, while the shoulder at 136 ppm and the peak at 129 ppm are associated with aromatic C atoms. The peak at 116 ppm from that in polyimide is broadened and merges with the peak at 129 ppm. This confirms that the bulk of CMS-500 retains some of the polymer structure in bulk materials, although effects of the pyrolysis are obvious. In CMS-550, the peak at 165 ppm has significantly broadened, it might be assigned as the C atom of C=O as well as the  $\alpha$ -C atoms associated with pyridinic N atoms; the shoulder at 138 ppm is attributed to the aromatic C atoms and the  $\alpha$ -C atoms associated with pyrrolic N atoms; the strong peak at 126 ppm is assigned to the graphene C and likely  $\beta$ -C atoms associated with pyridinic N atoms. In the CMS-675 and CMS-800 samples, only one broad peak was observed at 123 ppm and 119 ppm, respectively, which shows the typical  $^{13}\text{C}$ -NMR lineshape of graphene-type materials. This broad peak is assigned mainly to  $\text{sp}^2$  C of graphene, and also contribution from C atoms associated with pyrrolic N atoms as well as to  $\beta$ -C atoms associated with pyridinic N atoms.<sup>[9a]</sup> The aromatic  $\text{sp}^2$  carbon peak shifts to low ppm value and broadens simultaneously with increase of pyrolysis temperature in Figure 3d, indicates that higher pyrolysis temperatures lead to C atoms which mainly exists as graphenes form, where some C atoms are associated with pyridinic or pyrrolic nitrogen.

In Figure 4a, the polyimide exhibits several diffraction peaks at  $2\theta$  of 14.7, 19.7, 27.5, 29.4, 36.7, and 44.5°. These peaks also appear in CMS-500, which is in agreement with finding from FTIR and NMR results where it was concluded that the sample still maintained high degree of PI structure. The peaks disappeared in

the CMS-550, instead, a very broad peak with the center at about  $2\theta$  of 22.5° is observed. The WAXD pattern of CMS-550 is different from that of the CMS-675 and CMS-800 shown in Figure 4a. The CMS-675 and CMS-800 samples show similar patterns containing a main amorphous peak and an additional smaller peak, which is a typical WAXD patterns of CMS materials.<sup>[2e, 2i]</sup> The  $2\theta$  value of the main peak is 24.0° for CMS-675 and 24.8° for CMS-800, and the small peak at 44° remains unchanged. The calculated average interchain distances ( $d$ -spacing) values are therefore 3.95 Å (CMS-550), 3.70 Å (CMS-675), and 3.59 Å (CMS-800), respectively. This is in agreement with the  $d$ -spacing for a polymer char which can vary from 5 to 3.35 Å, depending on the extent of carbonization and atomic organization.<sup>[13]</sup> The decrease of  $d$ -spacing values with increasing pyrolysis temperatures reflects the decreased size of micropores and ultramicropores in CMS materials. The weak peak at about 44° demonstrates the  $d_{101}$  and/or  $d_{100}$  plane of carbon-carbon spacing on graphite-like planes.<sup>[13]</sup> This peak is more pronounced at a higher pyrolysis temperature, indicating a more ordered graphitic-like structure of the CMS materials.

Since CMS-500 is a mixture comprising mainly residual polymer with a few pyrolyzed components. To avoid unnecessary complexity and interference information in deconvolution of high resolution spectra, only the highly carbonized CMS-550, the more pure-carbon materials of CMS-675 and CMS-800 were investigated using Raman spectroscopy and XPS. Raman spectroscopy has been used to study carbonaceous materials, since it is nondestructive and sensitive to intrinsic defects of the graphitic lattice.<sup>[14]</sup>

A typical bimodal distribution of pores for CMSs were observed (Figure S2). Two apparent broad strongly overlapping peaks at  $\sim 1330\text{ cm}^{-1}$  and  $1560\text{ cm}^{-1}$  were observed for CMSs in Raman spectra. The G band ("Graphite") at about  $1560\text{ cm}^{-1}$  is analogous to the ideal graphitic vibration mode ( $E_{2g}$ -symmetry), the D (Defect) peak (graphene layer edges,  $A_{1g}$ -symmetry) at about  $1330\text{ cm}^{-1}$  is known as the characteristic for disordered graphite.<sup>[15]</sup> Different deconvolution of Raman spectra were

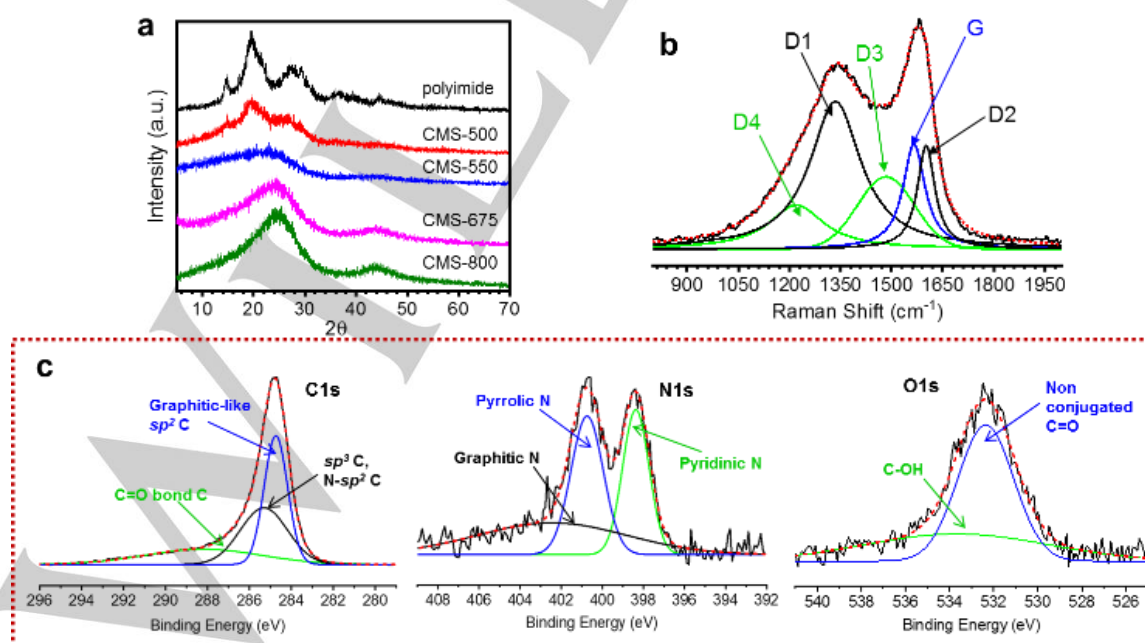


**Figure 4.** Characterization of CMS materials from  $^{15}\text{N}$  labeled PMDA/pDA polyimide: (a) WAXD, (b) typical Raman, and (c) typical XPS using CMS-675 as an example.

explored and the best fitting was achieved in this work (Figure 4b) with four Lorentzian functions for D1, D2, D4 and G, and one Gaussian function for D3 band.<sup>[14-15, 15c]</sup> The D1 band is due to a graphitic lattice vibration mode with  $A_{1g}$  symmetry; D2 band is generally assigned to graphitic lattice vibrations mode with  $E_{2g}$  symmetry, analogous to that of G band but involving isolated graphene layers, i.e., not directly sandwiched between two other layers; the D3 band originates from the amorphous carbon fraction, while the origin of the D4 band is still under debate, and both the D3 and D4 bands are usually found in highly disordered carbonaceous materials.<sup>[14-15, 15c]</sup> All of the CMS materials (Figure S3) are composed of highly disordered amorphous carbon (D3 and D4 bands), which is good agreement with XRD results. However, the CMS-550 shows obvious difference when compared to the CMS-675 and CMS-800. The D4 and D3 peaks are smaller, and shifted to higher frequencies for CMS-550. This is in agreement with observations from FTIR, NMR, and WAXD, which all provided evidence that the CMS-550 maintains a small amount of the polymer nature.

XPS is a useful tool to investigate elements within a depth up to about 5 nm from the surface of a materials. The XPS survey spectra indicated that all of the CMS materials exhibited three distinct peaks due to carbon, oxygen, and nitrogen. In order to study the detailed structure information on the surface of CMS materials, the C1s, N1s, and O1s peaks were deconvoluted into individual spectral lines, and the typical deconvolution is shown in Figure 4c. The binding energies and corresponding assignment to chemical species based on literature data of carbonaceous materials are summarized as follows:

C1s: 284.3~284.8 eV (graphitic-like  $sp^2$  carbon C=C, C-H), 285.0~286.7 eV (C-OH, C-O-C,  $sp^3$  hybridized C-C, N- $sp^2$  carbon N=C), 287.0~287.8 eV (C=O, O-C-O, quinone), 288.5~289.3 eV (O=C-OH, O=C-O-C, N- $sp^3$  carbon N-C), ~290.5 eV ( $\pi$ - $\pi^*$ , adsorbed CO and CO<sub>2</sub>).<sup>[15a, 15b, 16]</sup>

N1s: 398.1~399.3 eV (Pyridinic N); 399.8~400.3 eV (pyrrolic N); 400.6~401.2 eV (pyridonic N); 401.1~402.7 eV (graphitic N, including quaternary N – nitrogen substituents in aromatic graphene structures); 402.2~403.8 eV (pyridine-N-oxide); 404 eV (probably shake-up effects); >405 eV (chemisorbed nitrogen oxides).<sup>[15b, 16e-h, 17]</sup>

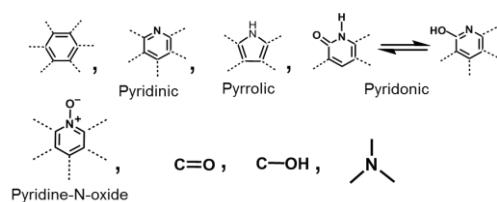
O1s: 530.1~531.3 eV (conjugated C=O, such as quinone groups); 531.1~532.1 eV (non-conjugated carbonyl groups, such as ketone, aldehyde, carboxyl C=O); 532.4~533.3 eV (-C-O-C); 533.5~534.7 eV (C-OH); > 535.0 eV (absorbed oxygen/water)<sup>[15a, 16d, 16f, 18]</sup>

Figure S4 shows deconvoluted C1s, O1s, and N1s peaks of CMS-550, CMS-675, and CMS-800. The C1s spectrum of each CMS could be deconvoluted into three peaks. The peak at a binding energy of ~284.7 eV is corresponding to graphitic-like  $sp^2$  C (C=C), C-C and C-H bonds. The peak at ~285.3 eV was labeled as “defects”, including C atoms at the edge of graphene-like layers, polyene connected to the edges, or carbon in structural defects within the graphene layers N- $sp^2$  C (N=C). And the peak at ~288.0 eV is assigned to C=O type bond C. No obvious variation was seen in the relative area of peaks of corresponding carbon types between CMS-675 and CMS-800. However, CMS-550 shows a slightly lower peak intensity at 287.3 eV while higher intensity at 285.0 eV, indicating a higher amount of “defects” as compared to other samples. These results indicate that analog C structures exists in the surface in all of the CMSs including CMS-550, CMS-675 and CMS-800. The O1s spectrum could be

deconvoluted into two peaks. CMS-550 showed a peak at 531.7 eV which can be assigned to O atoms in non-conjugated C=O groups including ketone, aldehyde, or carboxyl carbonyl moieties; another peak at 533.7 eV can be assigned to O atoms in C-OH structure. CMS-675 shows a main peak at 532.3 eV might due to O atoms in the non-conjugated C=O structure or C-O-C structure; similar to CMS-550, the peak at 533.8 eV is due to O atoms in the C-OH structure. The CMS-800 shows a predominant peak at 532.5 eV, while the peak of C-OH (533.7 eV) disappeared. This peak is due to O atoms in non-conjugated C=O structure or C-O-C structure; different from the other two samples, a small peak at 529.3 eV is detectable, which probably results from O atoms in conjugated C=O structures such as quinone groups. By comparing the O1s spectra of the three samples, it is evident that more oxygen atoms exist as C-OH structure in lower temperature pyrolyzed CMS materials. The N1s spectrum could be deconvoluted into three peaks. The peak at 398.2 ~ 398.6 eV corresponds to pyridinic N, the relative peak intensity decreases with increasing pyrolysis temperature, indicating that less pyridinic N exist in the higher temperature pyrolyzed CMS surface. This is probably due to the surface pyridinic N converted to graphitic N and cross-linked at higher temperature as will be discussed later. The peak at 400.3 ~ 400.8 eV is assigned as pyrrolic N and pyridonic N. Possibly CMS-550 contains only pyrrolic N (400.3 eV) while CMS-675 (400.7 eV) and CMS-800 (400.8 eV) contains a mixture of pyrrolic N and/or pyridonic N. It was found that both pyrrolic N and pyridinic N can convert to quaternary N during the pyrolysis of chars from polyacrylonitrile.<sup>[17d]</sup> The very broad peak centered at 401.1 eV in CMS-550 might be due to graphitic N, while the peak at 402.5~402.7 eV in CMS-675 and CMS-800 is assigned as graphitic N and some pyridine-N-oxide. The center position and relative intensity of this broad peak indicate that more graphitic and oxidized nitrogen structure exists in CMS pyrolyzed at higher temperature.

The above results indicate that the CMS materials do not contain perfect graphene plates of pure carbon atoms. Instead, during pyrolysis, the precursor PI forms carbon materials with a highly aromatic plate structure,<sup>[4]</sup> which contains also structural elements with various types of N, O, and H-containing functional groups on the surfaces and edges as well in the bulk. The N atoms exist as a heterocyclic structure such as pyridinic, pyrrolic, and graphitic nitrogen in all CMSs. In high temperature pyrolyzed CMS materials such as CMS-800 also pyridine N-oxide is found, i.e., high oxidized nitrogen structures occur at higher pyrolysis temperatures. The surface and edges of high temperature pyrolyzed materials contains more graphitic N and pyridine-N-oxides, while less pyridinic N is found. The O atoms exist as C-OH and C=O bonds in low temperature pyrolyzed CMS, while mainly as C=O and even N-O in high temperature pyrolyzed CMS. In other words, more oxygen atoms exist as C-OH structure in lower temperature pyrolyzed CMS materials. The N, O, and H atoms may exist in the bulk CMS materials, and also at the edges and defect sites in the graphene plates. The plate structure forms a “cell” structure within the CMS, with ultramicropores within the plates and micropores between plates, and “orphan strands” randomly packed between “cells”,<sup>[5]</sup> shown in Figure 1. The main structure of chemical species that assembled to CMS derived from PMDA/pPDA polyimide are listed in Scheme 1.

The pyrrolic N and pyridinic N were observed also in a complex copolyimide 6FDA<sub>1</sub>:BPDA<sub>1</sub>/DAM<sub>2</sub> during pyrolysis.<sup>[11]</sup> This



**Scheme 1.** Possible species in CMS materials.

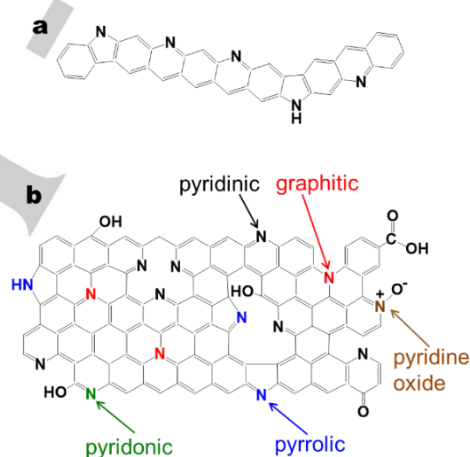
indicates that species in CMS materials from the simplest PMDA/pPDA polyimide appear in other polyimide-derived CMS materials. With temperature increases, part of the pyrrolic N and pyridinic N can convert to various forms of quaternary nitrogen.<sup>[17d]</sup> The aromatic ring can be cross-linked, for example, via aromatic radicals which are recombining to form “polymer carbon”.<sup>[19]</sup> Therefore, the strand fragments can be “cross-linked” through radical coupling and/or formation of graphitic nitrogen structures between strands, and possibly also through the release of N<sub>2</sub> from pyridinic N atoms between strands. A hypothetical schematic formation of graphitic nitrogen involving pyridinic and pyrrolic N is shown in Scheme S3.<sup>[17d]</sup> In addition to production of graphitic-like sp<sup>2</sup> carbons, the formation of pyrrolic and pyridinic N might be the initial products and basic intermediate for various N-containing structures in the pyrolysis process of polyimides.

Our earlier paper,<sup>[4]</sup> focused on conventional semi-flexible random coil PI precursors. For such precursors, a key element of such polyimide-derived CMS comprises rigid strands<sup>[4]</sup> shown in Scheme 2a. Plates formed from entropically driven assembly of such strands, like that in rigid liquid crystalline materials are envisioned to be key structures in such conventional CMS materials.<sup>[4]</sup> Conventional CMS materials appear to be created via the following steps:<sup>[4]</sup> (1) precursor PI aromatization with scissions at weaker backbone chain bonds to form rigid “strands” with different length and orientations; (2) the “strands” align and organize into imperfect “plates”; (3) the neighboring “plates” organize into “cell” structure, which is composed of ultramicropore slits between strands in a plate, micropores voids between “plate” walls, and “slit bypass pores” as the edge-imperfections between the neighboring ultramicroporous plates; (4) the adjacent micropore “cells” coalesce to create a “cellular” structure. Gas sorption and transport evidence also suggests “orphan strands”, not included in organized “plates” that are randomly packed between cells to form a continuous phase around “cells” in the “cellular” structure (Figure 1d). This continuous phase is expected to provide lower diffusion-selectivity but higher gas diffusivities. Penetrants may pass more easily through larger ultramicropores in the random continuous phase; however, local equilibrium exists between adjacent points, leading to overall desirable diffusion selectivity in the effective medium. Such a cellular structure is consistent with a mathematical model of sorption and transport within CMS materials derived from *conventional random coil polyimide precursors*.<sup>[5]</sup>

Additional components of graphene-like CMS plates might be mainly composed of such structures, together with fragments containing other possible structures represented in Scheme 2b. During pyrolysis process, highly aromatic rigid strands, i.e., the isolated strands (Scheme 2a) and fused fragments with analogous structures (Scheme 2b) can align and organize into the main plates. These plates may organize into imperfect “cells” containing micropores, with adjacent cells coalescing to yield the final cellular structure typical of conventional CMS materials.<sup>[4]</sup> Such amorphous CMS membranes contain micropores

connected via ultramicropores, providing intrinsic molecular sieve characteristics with attractive gas permeabilities. Graphene-like CMS “plates” are envisioned to be composed of isolated “strands” with pyridinic and/or pyrrolic rings at low pyrolysis temperature. Such feature, with few cross-linked fragments containing pyridinic, pyrrolic, graphitic structures, pyridonic, and few pyridine oxide structures provide high diffusion coefficients. **The chemical structures of strands in Scheme 2 depend on a variety of factors, namely precursor polymer structure, pyrolysis temperature, pyrolysis atmosphere, and inert purge gas flow rate. The diverse functional groups present can affect sorption affinity for specific gas molecules, but this is beyond the scope of the current study.**

The chemical structures of strands in Scheme 2 depend on a variety of factors, namely precursor polymer structure, pyrolysis temperature, pyrolysis atmosphere, and inert purge gas flow rate. Physically organized wall structures in Figure 1c based on Scheme 2a strand elements should be most prevalent at low pyrolysis temperatures. On the other hand, more fused structures in plate walls illustrated in Figure 1c similar to Scheme 2b should become more prevalent at higher pyrolysis temperatures. An isolated strand, even derived from the simplest PMDA/pPDA PI, contains pyrrolic moieties (Scheme 2a), preventing truly straight strands from the original precursor. This fortunate fact creates



**Scheme 2.** Possible fragments composed graphene-like plate structure in CMS materials pyrolyzed from PMDA/pPDA polyimide: (a) Isolated strands, and (b) Fused fragments.

useful ultramicropores between strands for molecular sieving in CMS “plates” formed from such strands during low temperature pyrolysis of any polyimide. As lateral connections develop between strands, the Scheme 2b features can become more prevalent in CMS formed from conventional random coil polyimide or PMDA/pPDA.

Increased pyrolysis temperature presumably alters the ultramicropores in both the continuous and distributed molecular sieving phase in Figure 1d derived from random coil precursors. This unique structure yields the CMS membrane molecular sieving properties with both high gas permeability/permeance and selectivity. High gas permeability of CMS membranes derived from various polyimides, summarized in our previous work appears consistent with this view.<sup>[20]</sup> Specifically, CMS-550 membrane from 6FDA<sub>1</sub>/BPDA<sub>1</sub>/DAM<sub>2</sub> showed a CO<sub>2</sub> permeability above 7000 Barrers with CO<sub>2</sub>/CH<sub>4</sub> selectivity around 29;<sup>[21]</sup> while the CMS-675 gives 1100 Barrers CO<sub>2</sub> permeability and CO<sub>2</sub>/CH<sub>4</sub> permeability of 66.<sup>[4]</sup>

Our results summarized below suggest the main chemical species in Scheme 1 appear to be present in both CMS derived

from conventional random coil PI precursors and those from the highly rigid PMDA/pPDA. Differences in sorption, diffusion and permeability properties of the two CMS types are quite interesting to compare and understand. As will be discussed below, such key performance properties differ dramatically, but can be understood using the dual mode sorption and transport models developed for CMS derived from random coil precursors.<sup>[5]</sup> First we consider the standard characterizations, and then focus on sorption, diffusion and permeability properties.

The CMS derived from a high performance conventional random coil PI precursor (6FDA<sub>1</sub>:BPDA<sub>1</sub>/DAM<sub>2</sub>) was used for comparison to the highly rigid PMDA/pPDA precursor. XPS, NMR, XRD, and Raman studies of CMS materials were done — as we did for PMDA/pPD precursor. Figure S5 shows that similar C1s and N1s, which were recorded in Figure S4 for CMSs from PMDA/pPDA, were detected for CMSs from 6FDA<sub>1</sub>:BPDA<sub>1</sub>/DAM<sub>2</sub>. The relative more complex O1s spectrum in Figure S5 reflects subtle O states derived from more complex 6FDA<sub>1</sub>:BPDA<sub>1</sub>/DAM<sub>2</sub> copolyimide. This indicates that CMS from 6FDA<sub>1</sub>:BPDA<sub>1</sub>/DAM<sub>2</sub> contains fragments like those for CMS derived from PMDA/pPDA. Figure S6 shows the <sup>13</sup>C DP/MAS NMR spectra of CMSs from different precursors, i.e., *PMDA/pPDA and 6FDA<sub>1</sub>:BPDA<sub>1</sub>/DAM<sub>2</sub> are composed of similar fragment species*. CMS-550 from 6FDA<sub>1</sub>:BPDA<sub>1</sub>/DAM<sub>2</sub> is identical to CMS-550 from PMDA/pPDA, except the shoulder at 138 ppm from the aromatic C atoms and the  $\alpha$ -C atoms associated with pyrrolic N atoms was not seen. This might be due to the relatively lower decomposition temperature of 6FDA<sub>1</sub>:BPDA<sub>1</sub>/DAM<sub>2</sub>. Note that this shoulder gets weaker at higher pyrolysis temperature in Figure S6. Compared with CMS-800 from PMDA/pPDA, the peak of CMS-800 from 6FDA<sub>1</sub>:BPDA<sub>1</sub>/DAM<sub>2</sub> is broader with movement to higher chemical shift. One of possibilities is due to slight conductivity of this sample. The observed lineshape is very typical for graphene—type materials containing a large amount of fused aromatic structures with little <sup>1</sup>H content. Our calculation also showed that the fused ring-system containing N cause higher chemical shift if the fused ring system contains OH or CO groups. Note that the shoulder at ~170 ppm indicates the presence of carbonyl moieties. This indicates possibly more fused fragments (Scheme 2b) in CMS-800 from 6FDA<sub>1</sub>:BPDA<sub>1</sub>/DAM<sub>2</sub>. Although the NMR results indicate that the precise chemical and spatial structure, as well as the concentration of a specific fragment species may differ between CMS materials, the Scheme 2 can reasonably represent CMS structures derived from other polyimides.

Similar to Figure 4a, a main peak at 2 $\theta$  value of ~24.0° and a small peak at ~44° were observed in WAXD for CMSs in Figure S7. Like Figure 4b and Figure S3, the Raman spectra of CMSs from 6FDA<sub>1</sub>:BPDA<sub>1</sub>/DAM<sub>2</sub> showed G band and D band (Figure S8). We also observed that the deconvolution of Raman spectra of CMSs varies based on polymer precursors and pyrolysis conditions.

We suggest, therefore, that for essentially all kinds of polyimides, the imide rings are likely to convert to pyridinic and/or pyrrolic rings which locate between the aromatic backbones of a dianhydride and a diamine, forming strands like Scheme 2a. Next, however, we consider implication of the random coil in conventional precursors versus the rigid rod PMDA/pPDA precursor. We presume the basic strand structure, like that in Scheme 2a, is initially formed in both cases; however, the absence of entanglements in PMDA/pPDA precursor can have key effects.

In fact, the “texture” or “morphology” of final CMSs appear to be strongly affected by the presence or absence of entanglements

in precursor polymer. Stresses at entanglements can cause scission at weak backbone links, thereby producing short mobile strands, rather than long, aligned strands, despite have similar chemical compositions showed above. This reality provides insight into why and how precursor polymers influence organization of “strands” in forming CMS “cell” structures for the polyimide precursor types. As shown below, gas sorption, diffusion and permeation behavior can be understood in CMS using this insight, with the PMDA/pPDA derived CMS providing a limiting case for CMS membranes from polyimides.

Unlike semiflexible polyimides such as 6FDA<sub>1</sub>:BPDA<sub>1</sub>/DAM<sub>2</sub>, which form random coil polymer chains with large free volume in a polymer membrane, the PMDA/pPDA has been found to possess only a rod-like conformation with limited rotational freedom.<sup>[22]</sup> PMDA/pPDA has a high inherent chain order along the chain axis with a high degree of in-plane orientation.<sup>[22]</sup> The high glass transition temperature (505 °C) as well as the very limited chain mobility (very high rigidity), make the fully rod-like PMDA/pPDA chain straight. Orientation in the film plane with a high degree of order also gives low free volume.<sup>[22-23]</sup> This morphology is consistent with both lower gas diffusion observed for PMDA/pPDA compared to other polyimides. PMDA/pPDA showed lower sorption than conventional polyimides (Figure S9). 6FDA<sub>1</sub>:BPDA<sub>1</sub>/DAM<sub>2</sub> has dramatically higher CO<sub>2</sub> permeability of 309 Barrers<sup>[24]</sup> while PMDA/pPDA only 1.0 ± 0.2 Barrers. Even H<sub>2</sub> (2.9 Å) showed permeability only 2.0 ± 0.1 Barrers with He/H<sub>2</sub> selectivity of 1.2 ± 0.1 in PMDA/pPDA precursor, emphasizing its impermeable nature. Such results reflect the rigid rod-like PMDA/pPDA chains that are oriented and tightly packed in multiple layer sheets in the plane of the *precursor film*.

The CMS-550 membrane from PMDA/pPDA showed a CO<sub>2</sub>/CH<sub>4</sub> selectivity of 34.8 ± 10.3, with a CO<sub>2</sub> permeability of only 396.3 ± 16.1 Barrers (vs > 7000 Barrers of 6FDA<sub>1</sub>:BPDA<sub>1</sub>/DAM<sub>2</sub> derived CMS). Moreover PMDA/pPDA derived CMS-800 had a CO<sub>2</sub> permeability of only 1.0 ± 0.1 Barrers (vs 1660 ± 236 Barrers of 6FDA<sub>1</sub>:BPDA<sub>1</sub>/DAM<sub>2</sub> derived) (Figure S10). Despite its impermeable nature, CMS from PMDA/pPDA showed remarkably high CO<sub>2</sub> sorption capacity, although lower than CMSs from 6FDA<sub>1</sub>:BPDA<sub>1</sub>/DAM<sub>2</sub> (Figure S11a). And the CO<sub>2</sub> sorption follows a dual mode shaped isotherm for CMSs from both precursors like that discussed for CMS derived from semiflexible precursors.<sup>[5]</sup> Clearly, despite similar species noted in Scheme 1 for both CMS types, permeation and diffusion properties reflect dramatic differences between 6FDA<sub>1</sub>:BPDA<sub>1</sub>/DAM<sub>2</sub> and PMDA/pPDA polyimides CMS “texture” or “morphology” features. Semiflexible entangled coil conventional polyimide precursors with large free volume can undergo stress-induced scissions at entanglement points to create relative shorter, randomly oriented “strands”. As discussed earlier, such strands can easily align to organize into “plate” and “cell” structures (Figure 1c) during the pyrolysis process. On the other hand, the oriented, non-entangled, rigid rod-like chains provide PMDA/pPDA with preexisting order to promote more or less stacked sheets. Evolution of CO, CO<sub>2</sub>, etc., during pyrolysis may expand inter-sheet spacing, but with minimal bond stress in the pyrolyzed PMDA/pPDA backbones (Figure S12). This fact should yield long rigid “strands” compared to random coil polyimides during pyrolysis. Such long “strands”, coupled with minimally disturbed spacings between stacked plates across a film (Figure 1c) in the direction of permeation, is consistent with extremely low penetrant diffusion coefficients, despite significant sorption capacity. In such a stacked

morphology, penetrants must execute more lateral jumps to encounter a suitable ultramicropore to enable movement in the direction of permeation. Such a structure is consistent with lower gas permeability (diffusion) in PMDA/pPDA derived CMS despite similar sorption capacities compared to CMSs derived from semiflexible coil polyimide precursors under the same pyrolysis temperature. On the other hand, these results imply that precursor with oriented, highly rigid chains may lower permeability of resulting CMS membranes. To get CMS membrane with high gas permeability, precursor polyimide with appropriate flexible backbone is essential. The PMDA/pPDA derived CMS is also found to be remarkably stable against physical aging (Figure S11b, Figure S13). This fact provides a view for designing copolyimide to make CMS membrane with inherent anti-physical aging properties. Furthermore, despite similar chemical compositions, sorption and diffusion properties are determined largely by CMS strand length, packing ability and arrangement into plates, and the lateral bonding between strands related to pyrolysis temperature. The PMDA/pPDA provides a “limiting” case that provides insight into polyimide-derived CMS materials.

## Conclusion

Specifically, while the permeability of the precursor polymer is well understood in terms of free volume, the permeability of CMS is best explained based on the textural structure due to assembled strands with different structures pyrolyzed from different precursor polyimides. Independent of the specific polyimide precursor, the concept of CMS “strands” (Scheme 2) created during aromatization of the precursor with similar chemical groups shown in Scheme 1 is useful. This fact notwithstanding, the shape and length of the aromatized “strand” affects detailed morphology of the resultant CMS. Introducing lower temperature removable bulk moieties like the CH<sub>3</sub> groups and the presence of intentional weaker bonds introduced in the polyimide backbone (-O-, biphenyl, etc.) are tools for CMS engineering. Transverse connection between strands may adjust distance between strands with permeable untramicropores, and could be influenced by polymer backbone natures, side functional groups, and final pyrolysis temperatures. A copolyimide might also create different “strands” and form “hybrid cellular” structure. The final CMS gas separation properties, can be understood in terms of precursor polyimide chemical structure using the ideas of “strands”, “plates”, and “cell” structures to move the CMS field forward. Such features are also helpful to understand aging and physical aging of CMS membranes. Related ideas may also guide development of CMS from non-polyimide precursors. Nevertheless, detailed work like that which has been done for polyimide precursors is needed for these alternative polymer families to see the degree to which such concepts can be transferred between precursor families.

## Acknowledgements

This work was supported by the U.S. Department of Energy Grant DE-FG02-04ER15510.

**Keywords** carbon molecular sieve • membrane • polyimide • structure • separation

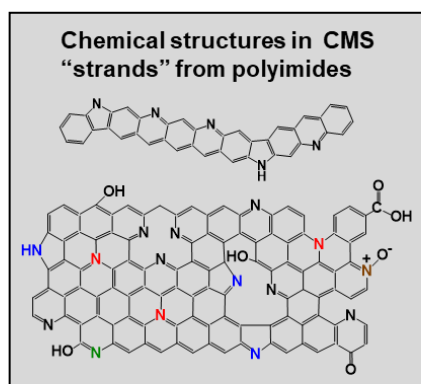
## REFERENCES

- aJ. Koresch, A. Soffer, *Journal of the Chemical Society-Faraday Transactions I* **1980**, *76*, 2457-8; bH. Hatori, Y. Yamada, M. Shiraishi, H. Nakata, S. Yoshitomi, *Carbon (New York, NY)* **1992**, *30*, 305-306; cJ.-i. Hayashi, H. Mizuta, M. Yamamoto, K. Kusakabe, S. Morooka, S.-H. Suh, *Industrial & engineering chemistry research* **1996**, *35*, 4176-4181; dH. Suda, K. Haraya, *Membrane Formation and Modification* **2000**, *744*, 295-313; eA. F. Ismail, L. I. B. David, *Journal of Membrane Science* **2001**, *193*, 1-18; fS. M. Saufi, A. F. Ismail, *Carbon* **2004**, *42*, 241-259; gM. Inagaki, N. Ohta, Y. Hishiyama, *Carbon* **2013**, *61*, 1-21; hY. Ma, M. L. Jue, F. Y. Zhang, R. Mathias, H. Y. Jang, R. P. Lively, *Angewandte Chemie-International Edition* **2019**, *58*, 13259-13265; iR. Swaidan, X. H. Ma, E. Litwiller, I. Pinnau, *Journal of Membrane Science* **2013**, *447*, 387-394.
- aD. Q. Vu, W. J. Koros, S. J. Miller, *Industrial & Engineering Chemistry Research* **2002**, *41*, 367-380; bK. M. Steel, W. J. Koros, *Carbon* **2005**, *43*, 1843-1856; cT. A. Centeno, J. L. Vilas, A. B. Fuentès, *Journal of Membrane Science* **2004**, *228*, 45-54; dL. R. Xu, M. Rungta, M. K. Brayden, M. V. Martinez, B. A. Stears, G. A. Barbay, W. J. Koros, *Journal of Membrane Science* **2012**, *423*, 314-323; eW. L. Qiu, K. Zhang, F. S. Li, K. Zhang, W. J. Koros, *Chemsuschem* **2014**, *7*, 1186-1194; fW. J. Koros, C. Zhang, *Nature Materials* **2017**, *16*, 289-297; gR. J. Swaidan, X. H. Ma, I. Pinnau, *Journal of Membrane Science* **2016**, *520*, 983-989; hC. Zhang, W. J. Koros, *Advanced Materials* **2017**, *29*; iZ. G. Wang, H. T. Ren, S. X. Zhang, F. Zhang, J. Jin, *Chemsuschem* **2018**, *11*, 916-923; jW. L. Qiu, J. Vaughn, G. P. Liu, L. R. Xu, M. Brayden, M. Martinez, T. Fitzgibbons, G. Wenz, W. J. Koros, *Angewandte Chemie-International Edition* **2019**, *58*, 11700-11703.
- aL. M. Robeson, *Journal of membrane science* **1991**, *62*, 165-185; bB. D. Freeman, *Macromolecules* **1999**, *32*, 375-380; cL. M. Robeson, *Journal of Membrane Science* **2008**, *320*, 390-400; dD. E. Sanders, Z. P. Smith, R. L. Guo, L. M. Robeson, J. E. McGrath, D. R. Paul, B. D. Freeman, *Polymer* **2013**, *54*, 4729-4761.
- M. Rungta, G. B. Wenz, C. Zhang, L. R. Xu, W. L. Qiu, J. S. Adams, W. J. Koros, *Carbon* **2017**, *115*, 237-248.
- O. Sanyal, S. S. Hays, N. E. León, Y. A. Guta, A. K. Itta, R. P. Lively, W. J. Koros, *Angewandte Chemie International Edition* **2020**, *59*, 20343-20347.
- S. S. Hays, O. Sanyal, N. E. Leon, P. Arab, W. J. Koros, *Carbon* **2020**, *157*, 385-394.
- aK. M. Steel, W. J. Koros, *Carbon* **2003**, *41*, 253-266; bH. O. Pierson, *Hand Book of graphite, diamond, and fullerenes*, Noyes New Jersey, **1993**.
- aM. J. Duer, *Solid state NMR spectroscopy: principles and applications*, John Wiley & Sons, **2008**; bD. C. Apperley, R. K. Harris, P. Hodgkinson, *Solid-state NMR: Basic principles and practice*, Momentum Press, **2012**.
- aS. Kuroki, Y. Hosaka, C. Yamauchi, *Carbon* **2013**, *55*, 160-167; bS. Kuroki, Y. Hosaka, C. Yamauchi, M. Sonoda, Y. Nabae, M.-a. Kakimoto, S. Miyata, *Journal of The Electrochemical Society* **2012**, *159*, F309-F315.
- S. Kuroki, Y. Nabae, M. Chokai, M.-a. Kakimoto, S. Miyata, *Carbon* **2012**, *50*, 153-162.
- J. S. Adams, A. K. Itta, C. Zhang, G. B. Wenz, O. Sanyal, W. J. Koros, *Carbon* **2019**, *141*, 238-246.
- J. C. Freitas, F. G. Emmerich, G. R. Cernicchiaro, L. C. Sampaio, T. J. Bonagamba, *Solid state nuclear magnetic resonance* **2001**, *20*, 61-73.
- G. M. Jenkins, A. Jenkins, K. Kawamura, *Polymeric carbons: carbon fibre, glass and char*, Cambridge University Press, **1976**.
- H. J. Seong, A. L. Boehman, *Energy & fuels* **2013**, *27*, 1613-1624.
- aP. Parent, C. Laffon, I. Marhaba, D. Ferry, T. Zhegu, I. Ortega, B. Chazallon, Y. Carpentier, C. Focsa, *Carbon* **2016**, *101*, 86-100; bH. Wang, T. Maiyalagan, X. Wang, *ACS Catalysis* **2012**, *2*, 781-794; cA. Sadezky, H. Muckenhuber, H. Grothe, R. Niessner, U. Pöschl, *Carbon* **2005**, *43*, 1731-1742; dA. C. Ferrari, J. Robertson, *Physical review B* **2000**, *61*, 14095.
- aS. Yumitori, *Journal of materials science* **2000**, *35*, 139-146; bT. Takahagi, A. Ishitani, *Carbon* **1984**, *22*, 43-46; cA. Wollbrink, K. Volgmann, J. Koch, K. Kanthasamy, C. Tegenkamp, Y. Li, H. Richter, S. Kämnitz, F. Steinbach, A. Feldhoff, *Carbon* **2016**, *106*, 93-105; dA. Puziy, O. Poddubnaya, R. Socha, J. Gurgul, M. Wisniewski, *Carbon* **2008**, *46*, 2113-2123; eM. Kozłowski, *Fuel* **2004**, *83*, 259-265; fS. Biniak, G. Szymański, J. Siedlewska, A. Świątkowski, *Carbon* **1997**, *35*, 1799-1810; gS. Zhao, Z. q. Shi, C. y. Wang, M. m. Chen, *Journal of applied polymer science* **2008**, *108*, 1852-1856; hZ. Zafar, Z. H. Ni, X. Wu, Z. X. Shi, H. Y. Nan, J. Bai, L. T. Sun, *Carbon* **2013**, *61*, 57-62; iF. Yin, S. Wu, Y. Wang, L. Wu, P. Yuan, X. Wang, *Journal of Solid State Chemistry* **2016**, *237*, 57-63; jJ. Riefl, M. Lublow, S. Anders, M. Tasbihi, A. Acharjya, K. Kailasam, A. Thomas, M. Schwarze, R. Schomäcker, *Photochemical & Photobiological Sciences* **2019**, *18*, 1833-1839.
- aR. Arrigo, M. Hävecker, R. Schlögl, D. S. Su, *Chemical communications* **2008**, 4891-4893; bR. Pietrzak, *Fuel* **2009**, *88*, 1871-1877; cD. Sebastián, M. J. Nieto-Monge, S. Pérez-Rodríguez, E. Pastor, M. J. Lázaro, *Energies* **2018**, *11*, 831; dJ. Pels, F. Kapteijn, J. Moulijn, Q. Zhu, K. Thomas, *Carbon* **1995**, *33*, 1641-1653.
- aM. E. Schuster, M. Hävecker, R. Arrigo, R. Blume, M. Knauer, N. P. Ivleva, D. S. Su, R. Niessner, R. Schlögl, *The Journal of Physical*

## RESEARCH ARTICLE

- Chemistry A* **2011**, *115*, 2568-2580; bS. Zhang, X.-y. Li, J. P. Chen, *Journal of colloid and interface science* **2010**, *343*, 232-238.
- [19] G. Ehlers, K. Fisch, W. Powell, *Journal of Polymer Science Part A-1: Polymer Chemistry* **1970**, *8*, 3511-3527.
- [20] W. Qiu, F. S. Li, S. Fu, W. J. Koros, *ChemSusChem* **2020**, *13*, 5318-5328.
- [21] M. Kiyono, P. J. Williams, W. J. Koros, *Carbon* **2010**, *48*, 4432-4441.
- [22] J. Seo, S. Y. Lee, W. Jang, H. Han, *Journal of Applied Polymer Science* **2003**, *89*, 3442-3446.
- [23] H. Lei, M. Zhang, H. Niu, S. Qi, G. Tian, D. Wu, *Polymer* **2018**, *149*, 96-105.
- [24] L. Liu, W. Qiu, E. S. Sanders, C. Ma, W. J. Koros, *Journal of Membrane Science* **2016**, *510*, 447-454.

## Entry for the Table of Contents



The chemical structure of "fragments" that composed CMS "strands" from varied polyimide precursors are similar, however, the "texture" or "morphology" structure is greatly affected by precursors, determining CMS membrane separation performance. The CMS properties can be tuned via control the "strands" structure, thereafter the "plate" and "cellular" structures, by designing precursor polymer chemical structure and pyrolysis conditions.